



Hydrological responses of three gorges reservoir region (China) to climate and land use and land cover changes

Yixin Sun¹ · Qiang Zhang² · Wenlong Song³ · Senlin Tang² · Vijay P. Singh^{4,5}

Received: 23 May 2024 / Accepted: 6 August 2024
© The Author(s), under exclusive licence to Springer Nature B.V. 2024

Abstract

Three Gorges Dam is the largest hydraulic infrastructure in the world, playing a pivotal role in flood mitigation. The hydrological responses of the Three Gorges Reservoir Region (TGRR) to climate change and human activities are unclear, yet critical for the Three Gorges Dam's flood control and security. We simulated streamflow and water depth by coupling the Variable Infiltration Capacity model and the CaMa-Flood model. Daily discharge at the outlet of TGRR was well modeled with a relative error within 2% and a Nash-Sutcliffe efficiency coefficient of approximately 0.81. However, the flood peak was overestimated by 2.5–40.0% with a peak timing bias ranging from 5 days earlier to 2 days later. Runoff and water depth in the TGRR increased from 2015 to 2018 but decreased during flood seasons. Land use and land cover changes in 2015 (LUCC2015) and 2020 (LUCC2020) were analyzed to quantify their hydrological impacts. During the 2015–2018 period, land use conversion increased in built-up areas (+0.6%) and water bodies (+0.1%), but decreased in woodland grassland (-0.7%) and cropland (-0.1%). This led to a slight increase in runoff and inflow of less than 4% across the TGRR, a 7.70% decrease in average water depth, and a 15.4% increase in maximum water depth. Water depths in the TGRR decreased during flood seasons, and increased during non-flood seasons. Increasing water depth was identified in northern TGRR. This study clarifies the historical TGRR's hydrological features under LUCC and climate changes, aiding regional flood mitigation in the TGRR.

Keywords Hydrological responses · Water depth · Runoff · Climate changes · LUCC · Three gorges reservoir regions

✉ Qiang Zhang
zhangq68@bnu.edu.cn

¹ Faculty of Geographical Science, Beijing Normal University, Beijing, China

² Advanced Interdisciplinary Institute of Environment and Ecology, Beijing Normal University, Zhuhai, China

³ China Institute of Water Resources and Hydropower Research, Beijing, China

⁴ Department of Biological and Agricultural Engineering and Zachry Department of Civil & Environmental Engineering, Texas A&M University, College Station, TX, USA

⁵ National Water and Energy Center, UAE University, Al Ain, UAE

1 Introduction

Increasing precipitation extremes under climate change amplified (Zhang et al. 2013; Myhre et al. 2019; Moustakis et al. 2021; Gründemann et al. 2022) flooding events globally (Jongman et al. 2012; Hirabayashi et al. 2013; Winsemius et al. 2016; Rodell and Li 2023). In recent years, there have been increasingly frequent floods in the Yangtze River (Jiang et al. 2008; Yu et al. 2009; Fang et al. 2018). To mitigate damage, various engineering measures have been implemented to reduce flood peaks. In the Yangtze River Basin (YRB), the Three Gorges Dam (TGD) and other mountainous reservoirs have been built for flood control. Among reservoirs located in the Yangtze River basin, Three Gorges Reservoir (TGR), with storage capacity of 39.3 billion m³, plays a critical role in flood mitigation (Zhang and Lou 2011; Xia and Chen 2021) (Fig. 1a). Floodwater in the Three Gorges Reservoir Region (TGRR) contribute from three sources: runoff from the TGRR itself, the drainage area upstream of the Cuntan station in the Yangtze River Basin, and runoff from the Wu River Basin. Tributaries within the TGRR contribute up to one-third of the total floodwater inflow from upstream to the TGRR. Moreover, runoff of the tributaries in the TGRR directly drains into the reservoir, significantly influencing reservoir security. Thus, investigating changes in hydrological characteristics of the TGRR is crucial for flood mitigation and security of the Three Gorges Dam.

Climate change and land use and cover change (LUCC) are the prime factors that impact hydrological processes of the TGRR (Zhang et al. 2015; Cheng et al. 2019; Wang et al. 2019a, 2020; Huang et al. 2020). Climate alters the temporal and spatial distribution of precipitation patterns, directly modifying flood regimes (Donat et al. 2016; Gründemann et al. 2022). Evapotranspiration (ET) is more likely to affect surface runoff (Zhou et al. 2013; Wang et al. 2019a). Meanwhile, LUCC alters hydrological processes by modifying transpiration, interception, and conservation (Hurkmans et al. 2009; Wang et al. 2015; Li et al. 2020). This is especially the case during urbanization, where a permeable vegetated land surface has been replaced by an impervious cityscape. This alteration affects the proportions of streamflow and baseflow, leading to increased velocity and flood risk (Zhou et al. 2013; Lin et al. 2022). The impervious area of the YRB increased by 162.46% from 1977 to 2018 (Luo and Zhang 2022). From 1990 to 2010, the forest and/or grass-based vegetation restoration project, namely the “Grain for Green” project since the 2000s, led to a 14% increase in vegetation cover from 1999 to 2009 in the YRB (Liu et al. 2014). The increasing vegetation cover leads to a decline in soil moisture and runoff due to increased ET and rainfall (Li et al. 2018), which causing reducing discharge in the YRB (Yang et al. 2015; Zeng et al. 2024). Therefore, the TGRR responses to compound impacts of urbanization and afforestation call for in-depth investigation.

Methods available for analyzing hydrological impacts can be grouped into three categories: catchment paired experiment, statistical analysis (Zhang et al. 2018a, b), and hydrological models (Zhang et al. 2015). The absence of observations renders the first two methods ineffective in the TGRR (Wang et al. 2011b). To better understand how hydrological processes change and recognize the impact of LUCC and climate change, hydrological models have been generally used (Hurkmans et al. 2009; Zhang et al. 2015; Wang et al. 2020; Gong et al. 2023). With the increased availability of remotely-sensed data, high-resolution meteorological data (Brookfield et al. 2023), hydrological model parameters, and

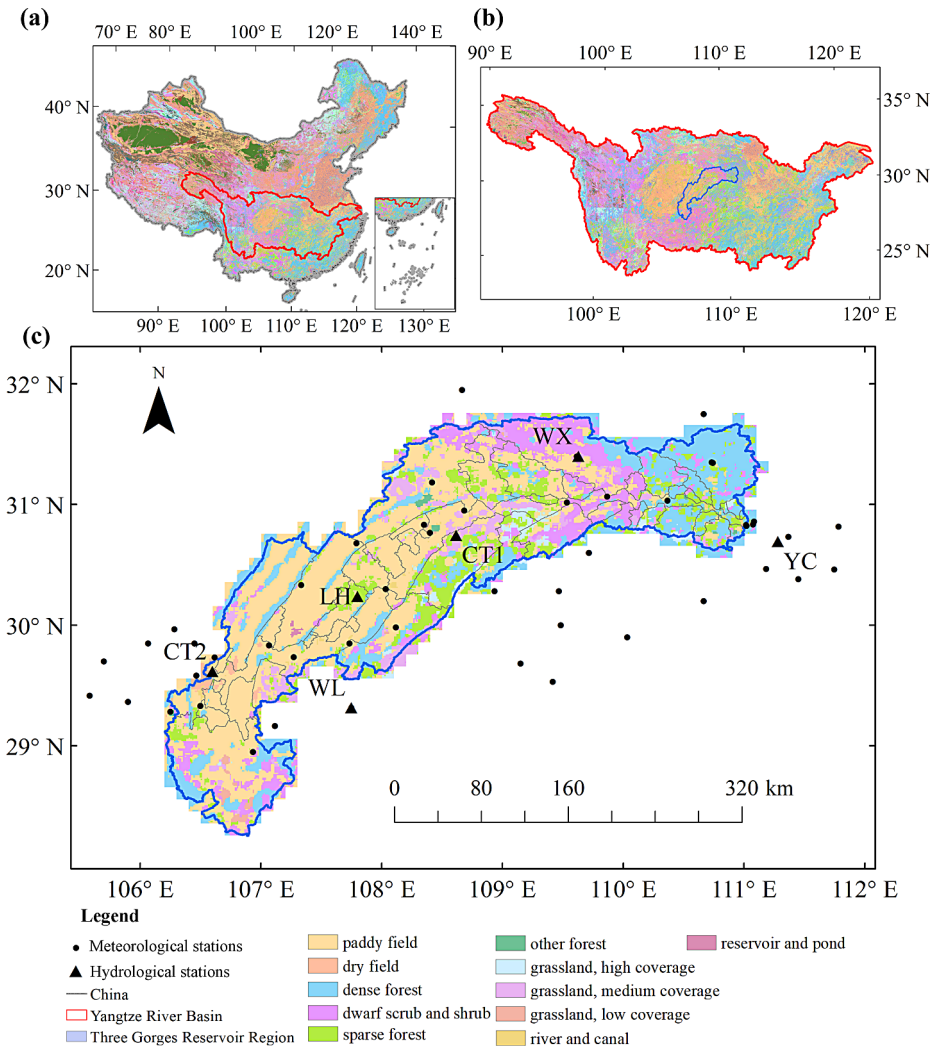


Fig. 1 Map showing the location of the Yangtze River Basin in China (a), the location of TGRR in the Yangtze River Basin (b), Map of the TGRR hydrological stations, and weather stations (c) The LUCC map is from the CNLUCC2015 dataset

high-quality input data are easier to access, enabling effective hydrological modeling (Sood and Smakhtin 2015).

In the TGRR, none of the rivers are hydrologically monitored over the entire tributary basins (Wang et al. 2011b). Evaluations of model parameters within the data-scare basin is an challenging task (Hrachowitz et al. 2013; Elmer et al. 2021). While there are streamflow observations at the outlet and the ungauged zone encompasses 70% of the area (Wang et al. 2011b). The scarcity of data challenges parameter estimation in hydrological modeling (Zhang et al. 2020). To implement hydrological modeling for simulation in ungauged areas, regionalization calibration method was used, and parameters were transferred from gauged

to similar ungauged sub-catchments (Alizadeh and Yazdi 2023). For example, parameters calibrated against to upstream observation at Poyang Lake were applied to non-measured area (Zhang et al. 2017).

Many studies of the YRB have analyzed monthly or annual streamflow observations to analyze the streamflow trend under climate change (Fang et al. 2018; Huang et al. 2024), and/or have evaluated the impact of human activities on streamflow (Zhou et al. 2013; Cheng et al. 2019; Wang et al. 2020). Previous studies on hydrological features in the TGRR used a lumped model without consideration of subbasin-specific hydrological responses (Jing et al. 2004). With the development of distributed hydrological models, these models have been widely used in flood flow modelling in the TGRR (e.g., GBHM, VIC, etc.) (Wang et al. 2011b, 2019b; Pang and Xu 2012). Very recent studies focused on integration of hydrologic and hydrodynamic models for flood flow modeling (Wang and Yang 2020; Xu et al. 2022). Distributed hydrologic models perform better in simulating rainfall-runoff processes at a large basin scale, whereas hydrodynamic models have higher modelling performance for smaller river basins. Combining these models allows for leveraging their respective strengths (Wang and Yang 2020). Previous studies simulated the flow and water depth in the TGRR by coupled XAJ hydrological model and one-dimensional hydrodynamic model (Wang et al. 2003; Zhang et al. 2020). Compared with the simulation results of a single hydrological model, the model coupled with XAJ and H1DM has a higher accuracy in the TGRR (Zhang et al. 2020). However, existing studies using one-dimensional hydrodynamic models only captured alterations at the outlet of the region, overlooking the spatial distribution of hydrological elements within the region. What's more, previous researches gave limited consideration to human activities like land use changes which are important factors in the hydrological cycle.

Using hydrological and hydrodynamic models, we attempted to simulate hydrological characteristics in the TGRR and tried to reflect water depth distribution of flood events. The study adopted the distributed hydrological model VIC with a physical mechanism to simulate the rainfall-runoff process under the conditions of complex topography and water system in the TGRR, and at the same time, the hydrodynamic model CaMa-Flood was applied with the VIC runoff results to reflect water depth distribution within the TGRR during the flood events. Based on the results, we analyzed the variations in hydrological elements within the historical period. Considering the impact of land-use changes on hydrological elements, we designed scenarios of land-use changes for different periods. We employed simulations to quantify the influence of land-use changes under various scenarios, exploring the impacts of both climate change and land-use changes on the hydrological feature in the TGRR.

2 Materials and methods

2.1 Study area

TGRR is in the upper Yangtze River (Fig. 1b), and specifically the stretch of the Yangtze River from Cuntan in the mainstream to the location near Wulong in the tributary, extending to the Three Gorges Dam (Shen et al. 2014). The Three Gorges Interval is located at the junction of Chongqing and Hubei provinces with drainage area of about 55,000km²,

and over 658 km in length. The altitude of the TGRR is between 3 and 3100 m. The TGRR exhibits an east-high-west-low topography, with Fengjie as the dividing point. Topography upstream to Fengjie is characterized by low hills and undulating landscapes. Regions downstream to Fengjie lies in the Three Gorges along the Yangtze River, including Qutang Gorge, Wuxia Gorge, and Xiling Gorge. TGRR is climatically characterized by monsoon area with annual rainfall ranging from 1000 mm to 1600 mm with 1200 mm on average. Rainfall from June to September accounts for more than 70% of the total annual rainfall, with frequent heavy rainfall events (Wang et al. 2011b).

Runoff in TGRR, upstream inflows from the Yangtze River, and the Wujiang River jointly constitute the three main sources of floods in the TGRR (Wang et al. 2011a). The main tributaries in the TGRR include 47 rivers, such as the Daning River, Xiangxi River, Xiaojiang River, Shennong River, Tangxi River, Meixi River, Zhuyi River, Modao River, Jiwanxi River and Ruxi River (Fig. 1c). The main tributaries with drainage areas exceeding 3,000 km² include the Yulin River, Longxi River, Xiaojiang River, MoDaoxi River, Daning River, and Xiangxi River.

2.2 Data

In this study, three kinds of input data were used: (1) meteorological forcing data; (2) vegetation and soil data; and (3) topographical data. Data required by the VIC model include the forcing elements of daily rainfall, temperature, and wind from 2015 to 2018 collected at 47 meteorological stations around the TGRR. The meteorological data was interpolated to each grid cell using the linear distance weighted interpolation method. Locations of the meteorological stations can be found in Fig. 1b. Daily discharges at six gauging stations from 2015 to 2018 were obtained from the Hydrological Yearbook of China, including Cuntan station (CT2, which measures the inflow from Yangtze River into the TGRR), Wulong station (measures the inflow from Wujiang River into the TGRR), Yichang station (the outlet of the TGRR), Lianghe station (LH, in the Quxi basin), Wuxi station (WX, in the Daning River basin), and Changtan station (CT1, in the Modao River basin). Daily water level data from 2015 to 2018 at Cuntan, Wanxian, Qingxichang, Shibanning, and Wuxi stations were also obtained from the Hydrological Yearbook of China.

The vegetation classification is derived from the 1 km land cover classification for 1992–1993 from the Advanced Very High-Resolution Radiometer (AVHRR) provided by the University of Maryland (Hansen et al. 2000). Table S1 lists the detailed land cover classes. The land use and cover data is based on China's Multi-Period Land Use Land Cover Remote Sensing Monitoring Data Set (CNLUCC) (Xu et al. 2018). This dataset with a spatial resolution of 1 km for the years of 1990, 1995, 2000, 2005, 2010, 2015, and 2020. Detailed land cover classes are listed in Table S2. Considering the study period of 2015–2018, the land-use data for 2015 and 2020 were utilized. The land cover map derived from AVHRR has been updated by incorporating the construction land class from the CNLUCC dataset, resulting in an updated LUCC dataset. Soil texture is based on the Harmonized World Soil Database (HWSD v1.21)(FAO/IIASA/ISRIC/ISSCAS/JRC 2012) from the FAO, offering detailed soil attributes for two soil layers.

The digital elevation model (DEM) of the catchment originates from GDEM v3 (ASTER Global Digital Elevation Map). The spatial resolution of the DEM is 30 m. This digital elevation model data set is used to extract the channel network. The MERIT Hydro dataset

(Yamazaki et al. 2019) is taken for river-floodplain parameterization river length, and river width data in the hydrodynamic models.

2.3 Models and method

The general procedures used for simulation and data processing are summarized in Fig. 2.

2.3.1 Models

The Variable Infiltration Capacity (VIC) hydrologic model is used in this study. The VIC model is a macroscale, semi-distributed land surface hydrologic model, which shares several basic features with other land surface models (LSMs) (Liang et al. 1994). The runoff generation scheme in VIC represents both saturation and infiltration excess runoff processes dynamically in a model grid cell through a statistical parameterization of sub-grid heteroge-

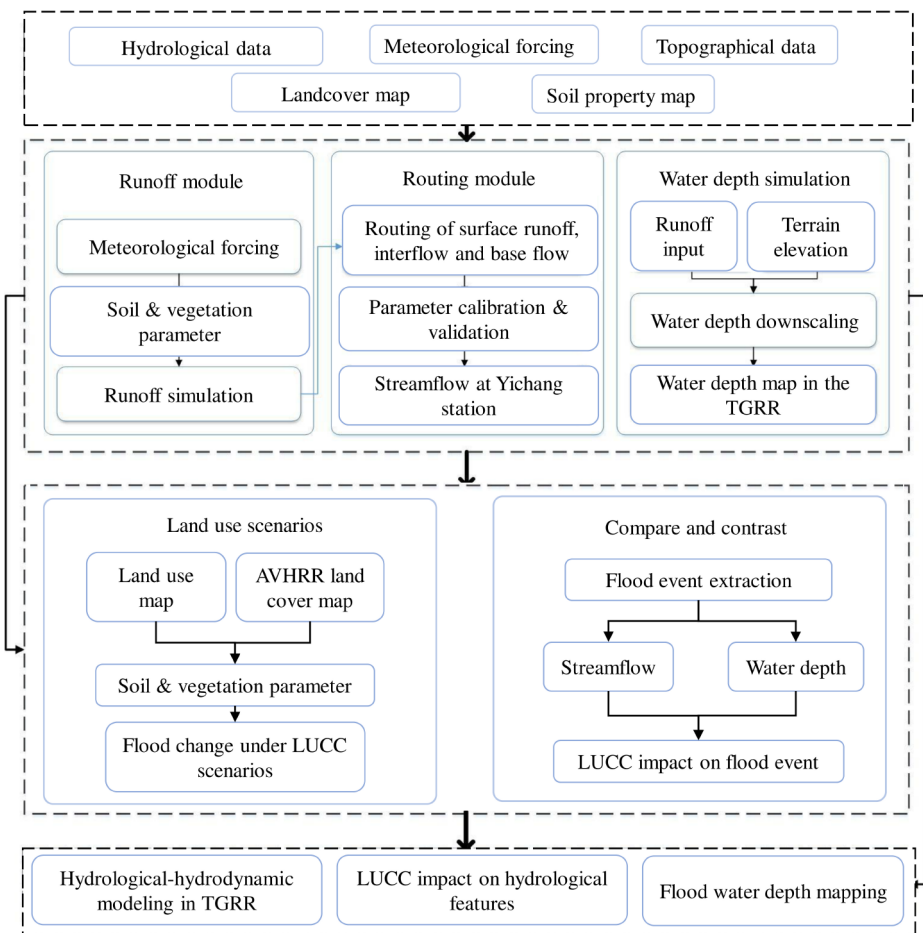


Fig. 2 Flowchart for methodology (four main components included: data used, simulation procedure, scenario design, and result analysis)

neity in terms of soil and rainfall (e.g., local water holding capacity) (Liang and Xie 2001). This led to better performance in runoff simulation. Runoff is comprised of surface runoff, subsurface flow (baseflow), and interflow. The VIC model has been successfully applied in YRB (Gu et al. 2015; Lu et al. 2018) and TGRR (Wang 2021). VIC 4.1.2 is used in this study. A separate surface routing model is coupled with the VIC model for routing (Lohmann et al. 1996). Utilizing the runoff output from the VIC model, this model generates daily streamflow output at the basin outlet.

CaMa-Flood is a hydrodynamic model and has been used for global- and basin-scale flood simulations (Hirabayashi et al. 2013; Willner et al. 2018; Wang et al. 2021). By parameterizing the subgrid-scale topography of a floodplain, it calculated simulated discharge, velocity, water level, and flood inundation depth by solving the local inertial equation, thus describing floodplain inundation dynamics (Yamazaki et al. 2011, 2013, 2014). The water level and flooded area are diagnosed from the water storage at each unit-catchment using the sub-grid topographic parameters of the river channel and floodplains (Yamazaki et al. 2011). The progression of water storage is determined by solving the water balance equation, taking into account the incoming water from upstream cells, the outflow to downstream cells, and the runoff input for each catchment unit (Yamazaki et al. 2011). Therefore, adopting the model could simulate changes in all stages of flooding, including discharge and water levels. The 1-min water depth data (about 2 km at the Equator) was obtained by downscaling based on DEM (Shin et al. 2020).

2.3.2 Coupled hydrological and hydrodynamic model

Utilizing Digital Elevation Models (DEMs), geographical data, and topographical features of the watershed, this study constructed the distributed hydrological model and the hydrodynamic model in the TGRR. Using these models, hydrological characteristics within the TGRR are simulated, including runoff, streamflow, and water depth. Initially, the VIC model was utilized to generate daily surface and subsurface runoff, including interflow and baseflow. Subsequently, the runoff produced by the VIC model served as the boundary condition for the CaMa-Flood model to calculate water depth.

Meteorological forcing data for the VIC model, including precipitation, temperature, and wind speed data, are sourced from 47 stations around the TGRR, as detailed in Sect. 2.2. These data were interpolated into 0.1 degrees using the inverse distance weighting method. Soil, vegetation, and land cover data that are necessary for the VIC model were detailed and described in Sect. 2.2 (Soil texture is based on HWSO, land cover data is from CNLUCC, and vegetation data is from the land cover classification from AVHRR). For this study, we ran the VIC model version 4.1.2 in water balance mode at a daily time step and at grid resolutions from 0.1 degrees. There are 637 grids in the TGRR. In this study, the routing model developed by Lohmann et al. (1996) is used to calculate the discharge at the basin outlet. The overflow employs the unit hydrograph method, while the channel routing employs the linear Saint Venant equations.

Taking the runoff simulation of VIC as forcing, CaMa-Flood runs daily with a spatial resolution of 0.1 degree. The water depth series is calculated from 2015 to 2018 with the first two years repeated as a spin-up period. The period 2015–2018 was chosen for this study because the meteorological station data and hydrological observation are accessible within

this period. The water depth is calculated based on water storage at each grid cell assuming hydro-geometry power-law equations (Yamazaki et al. 2014).

2.3.3 Model calibration and validation

Due to the scarcity of observation data, the real streamflow of the TGRR is not available, thus it is not possible to determine the parameter rate for the whole region based on the interval flow data. According to previous research (Xie et al. 2007), parameters in the TGRR are obtained following this procedure: model parameter is estimated from a limited number of calibrated basins and then regionalized to the whole region. It is noted that naturalized streamflow without reservoir regulation is simulated in this research, thus only hydrological stations without the backwater effects are selected, namely Lianghe hydrological station, Wuxi hydrological station, and Changtan hydrological station. Parameter estimation was performed at these hydrological stations during the periods 2015–2017 (the calibration period) and 2018 (the validation period). A trial and error calibration method is being used and the calibrated values (Park and Markus 2014; Ju et al. 2020) of Binf, Ds_Max, Ws, D2, D3 are shown in Table 1.

The parameters shown in Table 1 were estimated by calibration for the best fit of model outcomes to observed behavior. Five metrics were used to assess the model performance: Nash–Sutcliffe Efficiency (NSE), Relative error (Re), determination coefficient (R-square), Normalized Root Mean Square Error (RMSE), and Normalized RMSE (NRMSE). The formula for each indicator is given below (Eqs. (1)–(5)). The main evaluation metrics as the objective function are Re and NSE. Re reflects the total accuracy of the model simulation, and NSE reflects the fitness between the simulated flow and the observation. According to (Moriassi et al. 2007, 2015), model performance at the basin scale can be evaluated as satisfactory if daily RE < 25% and NSE > 0.5.

$$NSE = 1 - \frac{\sum (Q_{sim} - Q_{obs})^2}{\sum (Q_{obs} - \overline{Q_{obs}})^2} \tag{1}$$

$$Re = \frac{\overline{Q_{sim}} - \overline{Q_{obs}}}{\overline{Q_{obs}}} \tag{2}$$

Table 1 Calibrated parameters in the VIC model

Parameter	Range	Description	Unit
Binf	0–2	Variable infiltration curve parameter	None
Ds_Max	0–50	Maximum velocity of baseflow	mm/day
Ws	0–1	Fraction of the maximum soil moisture where nonlinear base-flow occurs	None
D2	0.1–1.5	Thickness of the second soil layer	m
D3	0.1–1.5	Thickness of the third soil layer	m

$$RMSE = \sqrt{\frac{\sum (Q_{obs} - Q_{sim})^2}{N}} \tag{3}$$

$$NRMSE = \frac{RMSE}{\max(Q_{obs}) - \min(Q_{obs})} \tag{4}$$

$$R^2 = 1 - \frac{\sum (Q_{sim} - Q_{obs})^2}{\sum (Q_{obs} - Q_{obs})^2} \tag{5}$$

To test the efficiency of the parameter regionalization result, a verification was conducted by comparing the observed flow at Yichang station and simulation results from 2015 to 2018. Located in the outlet of the TGRR, Yichang hydrological station has streamflow series data. Combined with the incoming water from Cuntan and Wulong hydrological stations and simulated runoff in the TGRR, simulated streamflow at the outlet of the TGRR is available.

2.3.4 Flood events extraction and validation

The study evaluates model efficiency in simulating flood events in TGRR by conducting verification on flood peak discharge and peak time.

Utilizing the Peaks Over Threshold method, this study applied a threshold of 25,000 m³/s to identify significant flood events based on observed streamflow data recorded at Yichang station from 2015 to 2018. However, the average flow from July to the end of August 2018 exceeded 25,000 m³/s, so a threshold of 40,000 m³/s was used. Therefore, we have not taken a uniform flood standard. A total of 10 flood events were extracted from 2015 to 2018 (Table 2 shows the list of flood events). Maximum discharge during a flood event is defined as the flood peak, and the occurrence time of the maximum flow during a flood event is defined as peak time. The study calculates the relative error between simulated discharge and observed values for flood peak and between simulated and observed peak times.

2.3.5 Analysis of changing hydrological features

To examine annual flow variations, this study computed the monthly averages, maximums, and minimums of discharge in the TGRR from 2015 to 2018, the statistical characteristics

Table 2 Extracted flood events in 2015–2018

Flood event No.	Flood duration		Observed peak flow(m ³ /s)
	Start date	End date	
1	2015/6/27	2015/7/7	31,400
2	2016/6/26	2016/7/6	33,100
3	2016/7/17	2016/7/20	26,700
4	2016/7/26	2016/8/7	31,300
5	2017/6/27	2017/6/30	27,100
6	2017/7/9	2017/7/25	29,900
7	2017/8/28	2017/9/2	26,600
8	2017/9/28	2017/9/30	25,100
9	2017/10/6	2017/10/17	29,800
10	2018/7/6	2018/7/18	43,600

of discharge and water depth series are listed in Table S3 (Burgan et al. 2013). Subsequently, linear trend analysis was performed on these monthly discharge series. To explore seasonal variations, the data were partitioned into flood season (May to October) and non-flood season (November to April). The same analysis has been performed on the water depth series.

2.4 Impact of LUCC on hydrological features

The land cover dataset from AVHRR (Hansen et al. 1999) has detailed vegetation information, while the CNLUCC has the latest built-up distribution data. To obtain input with detailed vegetation information and the latest land cover data in 2015 and 2020, we updated the built-up class in the AVHRR by land use type from CNLUCC. Then, we constructed the LUCC2015 and LUCC2020 scenarios and simulated the discharge and water depth under different LUCC scenarios. The analysis compared variations in discharge and water depth under different LUCC scenarios to assess the impact of diverse land uses on hydrological features in the TGRR.

At Yichang Station, flow patterns are impacted by both land use within the TGRR and the inflow from the upstream. To explicitly show the influence of land use changes on hydrological features in the TGRR, the discharge used for comparison involves routing exclusively based on local runoff without considering upstream inflow. Meanwhile, the water level simulated by the CaMa-Flood is still influenced by upstream inflow.

3 Results

3.1 Model calibration and validation

3.1.1 Parameter calibration

A list of parameters in the VIC model for each basin (Table S4) was identified. The metrics of simulated daily streamflow for those basins are shown in Table 3. The NSE between the observed and simulated streamflow at Wuxi station is above 0.6 during the calibration and validation periods, and the Re is below 20%. Moreover, this model performs better in the validation than in the calibration period. The NSE increased from 0.61 to 0.62, $|Re|$ decreased from 0.18 to 0.07, indicating that this model could provide satisfactory performances under out-of-sample situations. Based on the calibrated model from the Changtan hydrological station in the Modaoxi basin, the NSE value during the calibration period is below 0.5 and drops to 0.14 under the validation period with a $|Re|$ value of 1.21. According

Table 3 Performances of calibrated hydrologic models for both calibration and validation periods in three gauged basins

Hydrological stations	Period	NSE	Re	Rsquare	RMSE	NRMSE
Wuxi Stations (Daning basin)	Calibration Period	0.61	0.18	0.79	60.22	1.02
	Validation Period	0.62	0.07	0.80	67.34	1.03
Changtan Stations (Modaoxi basin)	Calibration Period	0.38	0.15	0.62	48.57	1.26
	Validation Period	0.14	1.21	0.52	30.16	1.53
Lianghe Stations (Quxi basin)	Calibration Period	0.31	7.33	0.61	5.71	2.33
	Validation Period	0.16	6.61	0.49	6.17	2.60

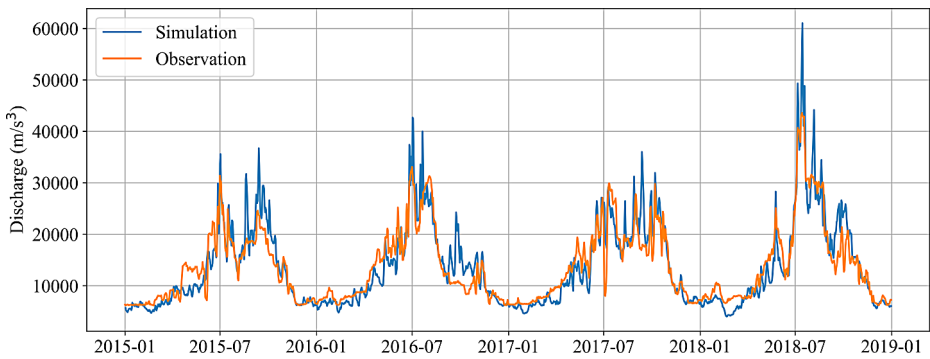


Fig. 3 Simulated versus measured streamflow in 2015–2018 at Yichang Station

to the calibrated model against the Lianghe hydrological station in the Quxi basin, the NSE value during the calibration period is 0.31 and drops to 0.16 under the validation period with a $|Re|$ value over 6.61. This indicates that the calibrated model in the Modaoxi and Quxi basins can hardly reflect the actual conditions of the region. The simulated and measured streamflow series from 2015 to 2018 at the Wuxi, Changtan, and Lianghe Stations are displayed in Fig. S1.

Previous studies (Moriasi et al. 2007, 2015) show acceptable model performance at the watershed scale if daily $Re < 25\%$ and $NSE > 0.50$. NSE values at the Changtan and Lianghe hydrological stations fall from 0.30 to 0.40. Additionally, the value of $|Re|$ at the Changtan station is approximately 1.00, whereas at the Lianghe station, it surpasses 6.00. Calibrated models underestimated the streamflow in the Quxi and Modaoxi basins (Fig. S1). The region is prone to recurrent short-duration intense rainfall events caused by strong convective weather. This poses challenges in accurately measuring precipitation of rain gauges, resulting in the underestimation of peak flow. Additionally, the lack of updated vegetation cover data adds to the biases in the model (Zhou et al. 2004; Wang 2021). Considering that only the calibrated model in the Daning River could reflect the actual conditions, parameters calibrated against the Wuxi hydrological station are regionalized to the TGRR.

3.1.2 Validation

Daily discharge at the outlet of the TGRR is well simulated with an NSE of 0.81, an R-square of 0.93, and Re of -2% (Fig. 3). 98 parameter sets with NSE values > 0.60 were adopted to evaluate the uncertainty of the parameters (Wang 2021) (Table S5). Results show that NSE ranges from 0.78 to 0.79, Re values range from -1% to -2%, and R-square is 0.92. Streamflow series under different parameter sets only results in marginal differences.

Qualitative comparison is performed between simulated water depth and observed water level data to access inaccessible reference datum data from hydrological stations. Under the effect of the TGD's backwater, the seasonal trend between observed and simulation was found at hydrological stations located at the mainstream. For the Shibanning station and Wuxi station, located outside the scope of the reservoir backwater effects, observed water level data aligns well with the trend of simulated water depth data, especially in the Wuxi station. Overall, the above qualitative comparison can reflect the credibility of the water

Table 4 Comparison between observed and simulated flood events characteristics

Flood event No.	Flood duration		Peak flow (m ³ /s)		Relative errors of flood peak flow (%)		Peak time		Errors in time to flood peak(d)	
	Start date	End date	Observed	Simulated	Observed	Simulated	Observed	Simulated	Observed	Simulated
1	2015/6/27	2015/7/7	31,400	35,579	13.3%		2015/7/1	2015/7/2	1	
2	2016/6/26	2016/7/6	33,100	42,674	28.9%		2016/7/1	2016/7/2	1	
3	2016/7/17	2016/7/20	26,700	33,567	25.7%		2016/7/18	2016/7/17	-1	
4	2016/7/26	2016/8/7	31,300	29,728	-5.0%		2016/8/3	2016/7/29	-5	
5	2017/6/27	2017/6/30	27,100	27,128	0.1%		2017/6/29	2017/6/27	-2	
6	2017/7/9	2017/7/25	29,900	29,163	-2.5%		2017/7/11	2017/7/10	-1	
7	2017/8/28	2017/9/2	26,600	31,214	17.3%		2017/8/31	2017/8/28	-3	
8	2017/9/28	2017/9/30	25,100	28,423	13.2%		2017/9/28	2017/9/30	2	
9	2017/10/6	2017/10/17	29,800	31,925	7.1%		2017/10/7	2017/10/7	0	
10	2018/7/6	2018/7/18	43,600	61,042	40.0%		2018/7/14	2018/7/15	1	

depth simulation results to a certain extent. Detailed information on water depth validation is in Supplementary Text 1 and Fig. S2.

According to Table 4, the relative error between simulated and observed peak flows ranges from -2.5 to 40.0% . Simulations mostly overestimated the peak flows, which may be influenced by the storage of hydraulic projects and water withdrawals (The TGRR has numerous water withdrawal sites, dams, and small hydropower stations). Bias in flood peak time ranges from 2 to -5 days. Notably, the bias is more pronounced for flood events in August, exceeding three days in deviation. This discrepancy may be attributed to the fact that August falls within the primary flood season in the TGRR (Yu et al. 2009), being characterized by intermittent rainfall. The overall high flow during this period could result in misjudgments of flood peaks.

3.2 Changing flood characteristics

3.2.1 Streamflow in 2015 to 2018

The monthly average, maximum, and minimum flow at the Yichang station increased from 2015 to 2018 (Fig. 4). Among them, the monthly maximum flow increased most significantly with a rising rate of $1808.28 \text{ m}^3/\text{s/a}$, followed by the monthly average flow of $1218.12 \text{ m}^3/\text{s/a}$. The least significant was the monthly minimum flow ($751.44 \text{ m}^3/\text{s/a}$). This is in line with the changes in the observed flow (Pang et al. 2022). According to observation, the monthly maximum flow rose at $1498.32 \text{ m}^3/\text{s/a}$, followed by the monthly average flow of $1065.48 \text{ m}^3/\text{s/a}$. Monthly minimum flow with a least increase rate of $667.44 \text{ m}^3/\text{s/a}$.

In 2015–2018, long-term monthly maximum streamflow is $36858.15 \text{ m}^3/\text{s}$, deviating by 3.95% from observation; multi-year monthly minimum streamflow is $5483.88 \text{ m}^3/\text{s}$, deviating by -12.61% from observation; and multi-year average streamflow is $13694.56 \text{ m}^3/\text{s}$, deviating by -0.06% from observation. In January, the average flow is the smallest at $6,275.36 \text{ m}^3/\text{s}$, deviating -11.61% from the observed value. Conversely, in July, the average flow is the largest at $27,240.81 \text{ m}^3/\text{s}$, with a deviation of 3.77% from the measured value. The monthly average flow exhibits a seasonal trend, initially rising and declining throughout the year, aligning with observations at Yichang station in the Yangtze River Basin. Rainfall, predominantly occurring in summer and autumn, is the prime driver for streamflow (Yu et al. 2009).

Streamflow during flood seasons increased from 2015 to 2018, and the increase rates of monthly average, maximum, and minimum flow were $1613.82 \text{ m}^3/\text{s/a}$, $2002.80 \text{ m}^3/\text{s/a}$, and $1175.46 \text{ m}^3/\text{s/a}$, respectively. The observed discharge displayed an increasing trend with rates ranging from $775.92 \text{ m}^3/\text{s/a}$ to $1542.78 \text{ m}^3/\text{s/a}$, and the most notable surge occurred in the monthly maximum flow of $1542.78 \text{ m}^3/\text{s/a}$, aligning with the simulation results. Streamflow in non-flood seasons also increased, however, the monthly minimum flow decreased. In the 2015–2018 (November–April) monthly average, maximum discharge showed an increasing trend during the non-flood season, with an increasing rate of $207.00 \text{ m}^3/\text{s/a}$ and $480.12 \text{ m}^3/\text{s/a}$. Minimum flow series showed a decreasing trend, with a rate of $-13.80 \text{ m}^3/\text{s/a}$. According to observation, measured data showed that the monthly discharge during non-flood season showed an increasing trend with an increasing rate varying between $192.78 \text{ m}^3/\text{s/a}$ to $392.22 \text{ m}^3/\text{s/a}$.

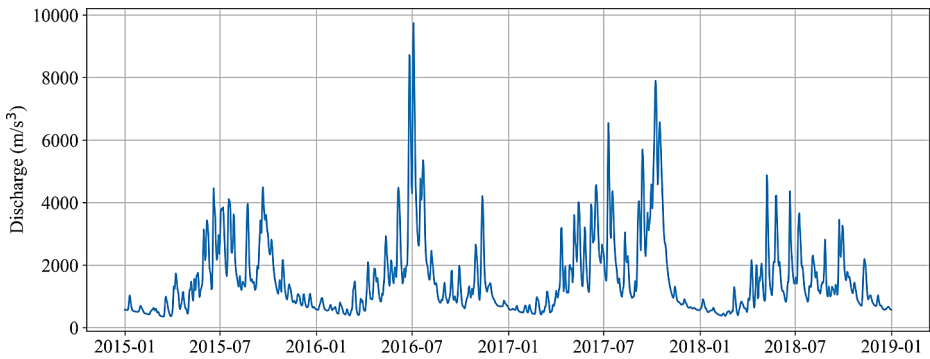


Fig. 4 Streamflow series at the outlet of the TGRR from 2015 to 2018 (inflow from upstream is excluded)

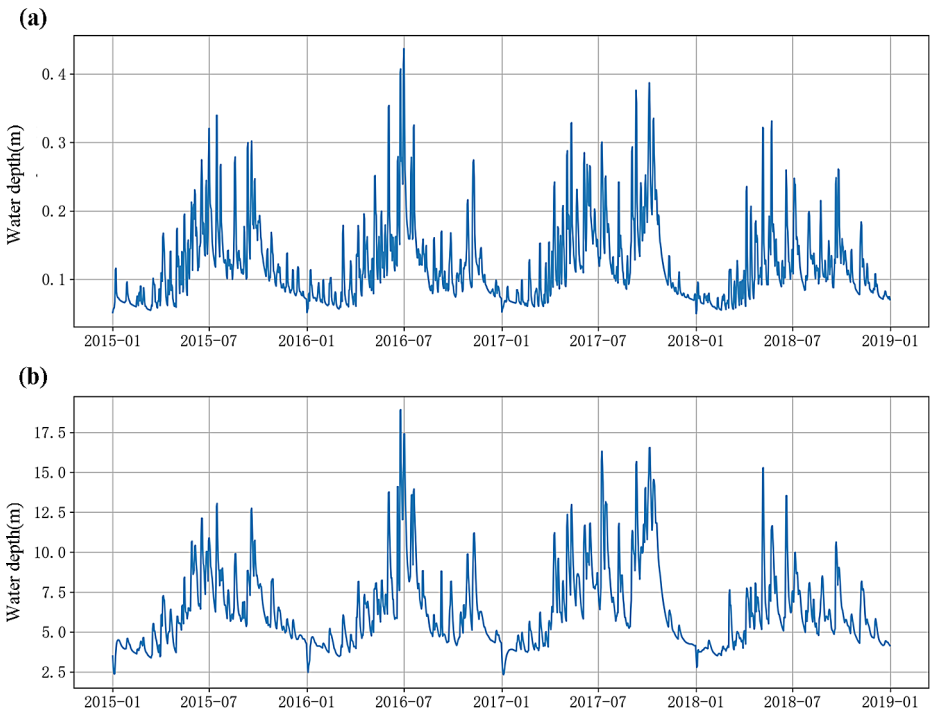


Fig. 5 (a) Mean water depth series from 2015 to 2018 in the TGRR, (b) The maximum water depth series from 2015 to 2018 in the TGRR

Discharge without the upstream inflow was also analyzed, and monthly mean maximum and minimum flow increased from 2015 to 2018 (Fig. 4). Increasing rates of monthly average, maximum, and minimum flow were $124.56 \text{ m}^3/\text{s/a}$, $34.92 \text{ m}^3/\text{s/a}$, and $8.40 \text{ m}^3/\text{s/a}$, respectively. Monthly mean maximum and minimum flow during non-flood season showed a decreasing trend, with decreasing magnitude of $-146.47 \text{ m}^3/\text{s/a}$, $-127.20 \text{ m}^3/\text{s/a}$, and $-87.60 \text{ m}^3/\text{s/a}$, respectively. In contrast, monthly mean maximum and minimum flow during flood season showed an increasing trend, with rates ranging from $40.44 \text{ m}^3/\text{s/a}$ to $191.76 \text{ m}^3/\text{s/a}$.

Therefore, incoming flow to the TGR increased continuously from 2015 to 2018, while minimum flow during the non-flood season decreased. The inflow is seasonally varied, with the average flow increasing from January to July and then decreasing, which is consistent with observation. Runoff within the region increased in 2015–2018 and decreased during flood season.

3.2.2 Water depth in 2015 to 2018

From 2015 to 2018, the average water depth in the TGRR increased, with maximum, minimum, and average values of 0.44 m, 0.05 m, and 0.12 m, respectively. (Fig. 5(a)). The changing rates of water depths during this period were 0.16 cm/a, 0.47 cm/a, and 0.11 cm/a for the maximum, minimum, and average water depth, indicating a consistent upward trend (Pang et al. 2022). However, the monthly average water depth in the TGRR interval during the flood season (May–October) decreased. The decreasing rate in the monthly maximum water depth is the highest (−0.61 cm/a), followed by monthly average water depth (−0.48 cm/a) and monthly minimum water depth (−0.21 cm/a). Water depths exhibit two peaks, occurring in July and October, respectively. In 2017, the average water depths within the region in the autumn flood events exceeded those in the summer flood events. The monthly average water depth during the non-flood event showed an increasing trend, with the most significant rise in the monthly maximum water depth at 0.60 cm/a. Following this, the monthly average water depth increased by 0.33 cm/a, and the monthly minimum water depth increased by 0.17 cm/a.

The maximum, minimum, and average values of the maximum water depth in the TGRR from 2015 to 2018 were 18.92 m, 6.39 m, and 2.33 m (Fig. 5(b)). The rising rate ranges from 0.34 m/a to 0.08 m/a. As the average water depth in the region, the maximum water depths within the region during the autumn flood events exceeded those in the summer flood events in 2017. The maximum water depth in TGRR was the highest in 2016. Monthly maximum water depths decreased during flood seasons, with changing rates of −0.11 m/year, −0.10 m/year, and −0.15 m/year for the monthly maximum, minimum, and average water depth. The total water depth in the TGRR during non-flood season shows an opposite trend, with the highest decreasing magnitude of monthly minimum water depth.

3.3 LUCC's effect on hydrological features

3.3.1 Land use/cover change

The land use types in the TGRR were mainly woodland grassland, grassland, grassland, and cropland types (Fig. 5). In 2015, there were 29 sub-basins where the primary land cover type was cropland (mainly found in the north and northeast regions), 10 sub-basins with woodland grassland, and the rest 9 sub-basins with woodland (mainly found in the south and southwest region). From 2015 to 2020, the main land cover types changed in the Zhuyihe, Changtanghe, and Baolonghe basins. The primary land use type of the Baolonghe basin changed from arable land to woodland grassland, the opposite change occurred in the Zhuyihe basin, and the main land use type of the Changtanghe basin changed from arable land to urban and buildings. Land cover proportions in the TGRR in different periods are shown in Table S6.

Land-use changes from 2015 to 2020 in the TGRR are shown in Fig. 6. The percentage of evergreen needles, deciduous broadleaf, mixed forests, and woodland remains the same from 2015 to 2020, at 4.2%, 2.9%, 2.2%, and 9.6%, respectively. Urban and built-up areas expanded evidently, increasing from 1.0% in 2015 to 1.6% in 2020. This growth includes a notable conversion of 42.9% from cropland and around 6.0% from grassland, mainly in the southwest region, encompassing basins like Wubuhe, Lixiangxi, Changranhe, and Chaoyanghe. The percentage of water bodies increased from 0.3% in 2015 to 0.4% in 2020, with growth occurring around the mainstream of the Yangtze River and Longxihe basin, mainly from cropland (94.7%) and grassland (5.3%). The percentage of grassland has seen a marginal increase from 6.9% in 2015 to 7.0% in 2020. This is mainly attributed to the conversion from cropland, predominantly occurring in the mainstream and northern watersheds (such as Qianjiang, Yuling, Xijiang, and Tangxi Basin).

Remote sensing data suggested that woodland grassland, cropland, and forest had been decreasing. The proportion of woodland-grassland within the TGRR declined from 18.6 to 17.9%, marking the most significant relative decrease. The loss of woodland grassland was mainly converted into Cropland, which occurred in the Qixianjiang, Jiuwangxi, and Dan-

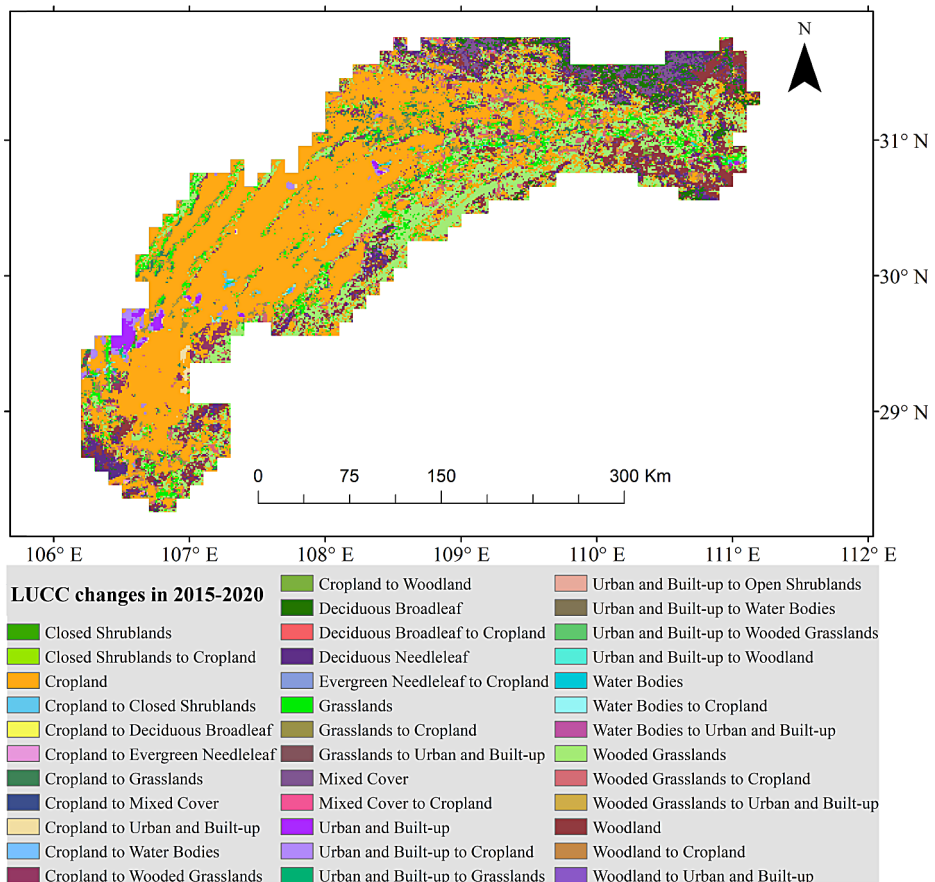


Fig. 6 LUCC transfer map of region for 2015–2020

ing basins. Cropland decreased from 54.2% in 2015 to 54.1% in 2020. The main types of diversion from cropland are woodland prairie and grassland, concentrated in the Xiaojiang, Tangxi, Meixi, Daning, and Modaoxi basins. At the same time, forest, woodland grassland, and grassland were mainly converted into cropland.

3.3.2 LUCC impact on discharge

The multi-year annual average flow at Yichang station is 13596.6 m³/s under the 2020LUCC scenario, which is slightly higher than that under the 2015LUCC scenario (13593.3m³/s). The multi-year annual maximum flow is 51171.5m³/s under the 2020LUCC scenario, which is higher than that under the 2015LUCC scenario (51165.5m³/s). Therefore, the streamflow variation at Yichang station across different land use scenarios is not discernable. The disparity in average annual flow remains within 5.00 m³/s, while the difference in maximum annual flow is limited to 8.00 m³/s.

Comparison of the discharge excluding upstream inflow under different scenarios shows that land use changes have a greater impact on discharge during the flood season. In flood season, variations in mean flow between different LUCC scenarios ranged from 3.70 to 7.80%, while the maximum flow differences ranged from 5.70 to 8.50%. In non-flood season, variations in mean flow between different LUCC scenarios ranged from 0.50 to 2.20%, while the maximum flow differences ranged from 0.70 to 2.88%.

Differences in monthly average and maximum flows under LUCC scenarios during the flood seasons (from May to October) in 2015–2018 are shown in Table S7. Notably, the most significant difference occurred in July, surpassing 8%. Nevertheless, regional runoff disparities and discharge at the outlet of the TGRR between land use scenarios remain relatively modest, all falling below 12.00 m³/s, with relative differences amounting to less than 4%. The results indicate that land use changes contribute to increased runoff in the TGRR, leading to a rise in the inflow of the TGR. However, the impact is relatively limited compared to factors like rainfall.

3.3.3 LUCC impact on water depth

Under LUCC2015 scenario, daily mean water depth in the TGRR ranged from 0.05 m to a maximum of 0.44 m from 2015 to 2018, with a multi-year average of 0.13 m, and notably higher values in 2016. Under the LUCC2020 scenario, the daily mean water depth in the TGRR remains within the same range as that in the LUCC2015 scenario, with a multi-year average of 0.12 m and notably higher values in 2016. This may be explained by the extreme precipitation in 2016 within the TGRR, leading to severe flooding in the middle and lower reaches of the Yangtze River. Between LUCC2015 and LUCC2020, the maximum mean water depth in the TGRR area remained stable, while the multi-year average decreased by 7.70%.

Under LUCC2015 scenario, daily maximum water depth in the TGRR ranged from 2.35 m to a maximum of 19.09 m from 2015 to 2018, with a multi-year average of 6.49 m and notably higher values in 2016. For LUCC2020 scenarios, daily maximum water depth ranged between 2.33 m and 18.92 m from 2015 to 2018, averaging 6.39 m over the multi-year span. The same as LUCC2015 scenario, the daily maximum water depth was higher in 2016 than in other years under the LUCC2020 scenario. In the LUCC2015 scenario, the

maximum water depth in the TGRR was 8.91% lower than that in the LUCC2020, while the average value displayed a 15.4% increase.

Table 5 shows seasonal variation in average and maximum water depth difference between LUCC scenarios. During flood seasons, water depth difference ranges from -0.35% ~ -3.53% in average value and -0.33% ~ -2.58% in maximum value. During non-flood seasons, water depth difference ranges from -1.38% ~ -2.86% in average value and -1.04% ~ -2.47% in maximum value. Reduction in water depth due to LUCC was more pronounced in March-June when the relative change rate in mean value exceeded 2% in absolute terms.

In the LUCC2015 scenario, the average water depth in the region was 0.02–0.58 cm lower than that in the LUCC2020. For the maximum water depth, the difference is 0.40–11.38 cm. The difference in water depth between the LUCC2015 and LUCC2020 scenarios shows evident spatial variations. Compared with LUCC2015 scenarios, the overall water depth in the region increased during flood events 1, 2, 5, and 10 in the LUCC2020 scenarios, while it demonstrates contrasting change during flood events 4, 7, and 8. Notably, for flood events 3, 6, and 9, water depth in the Daning basin exhibited an apparent increase, although the overall water depths still decreased. Land cover changes led to over 0.4 cm increase in mean water depth during flood events 1, 2, and 10. In LUCC2015 scenarios, maximum water depth surpassed by over 1 cm in flood events 3, 4, 6, 7, 8, and 9 compared with LUCC2020, with the most significant difference observed in flood6, exceeding 11 cm. Based on this classification, this section analyzes water depth differences due to different land use scenarios for Flood Events 1, 7, 8, and 9 (Fig. 7), with water depth differences for the remaining flood events plotted in Fig. S3.

In LUCC2015 scenarios, the average water depth was reduced by 0.58 cm (-1.73%) in flood event 1 (peaked on 07/01/2015) compared with LUCC2020, and the maximum water depth was 0.37% higher. In the north and northeast regions, there is an apparent reduction in water depth. The reduction in water depth takes over a 10 cm reduction in the river section from Cuntan Station to Qingxi Station in the mainstream of the Yangtze River and the Xiaojiang basin. In the midsection of the region, the difference in water depth is less pronounced between different scenarios.

Table 5 Comparison of monthly average and maximum water depth across multiple years under the 2015LUCC and 2020LUCC scenarios

Month	Average water depth(m)		Relative change (%)	Maximum water depth (m)		Relative change (%)
	2015LUCC	2020LUCC		2015LUCC	2020LUCC	
1	0.074	0.073	-1.86%	3.927	3.870	-1.45%
2	0.071	0.070	-2.38%	4.152	4.077	-1.83%
3	0.083	0.081	-3.26%	4.601	4.487	-2.47%
4	0.122	0.118	-2.86%	6.393	6.263	-2.03%
5	0.157	0.152	-3.53%	7.836	7.634	-2.58%
6	0.185	0.179	-3.20%	9.059	8.837	-2.44%
7	0.175	0.172	-1.85%	9.185	9.046	-1.51%
8	0.127	0.127	-0.47%	6.566	6.544	-0.33%
9	0.160	0.160	-0.35%	7.931	7.918	-0.17%
10	0.148	0.147	-0.74%	7.452	7.420	-0.43%
11	0.111	0.109	-1.38%	6.001	5.938	-1.04%
12	0.082	0.081	-1.41%	4.654	4.599	-1.17%

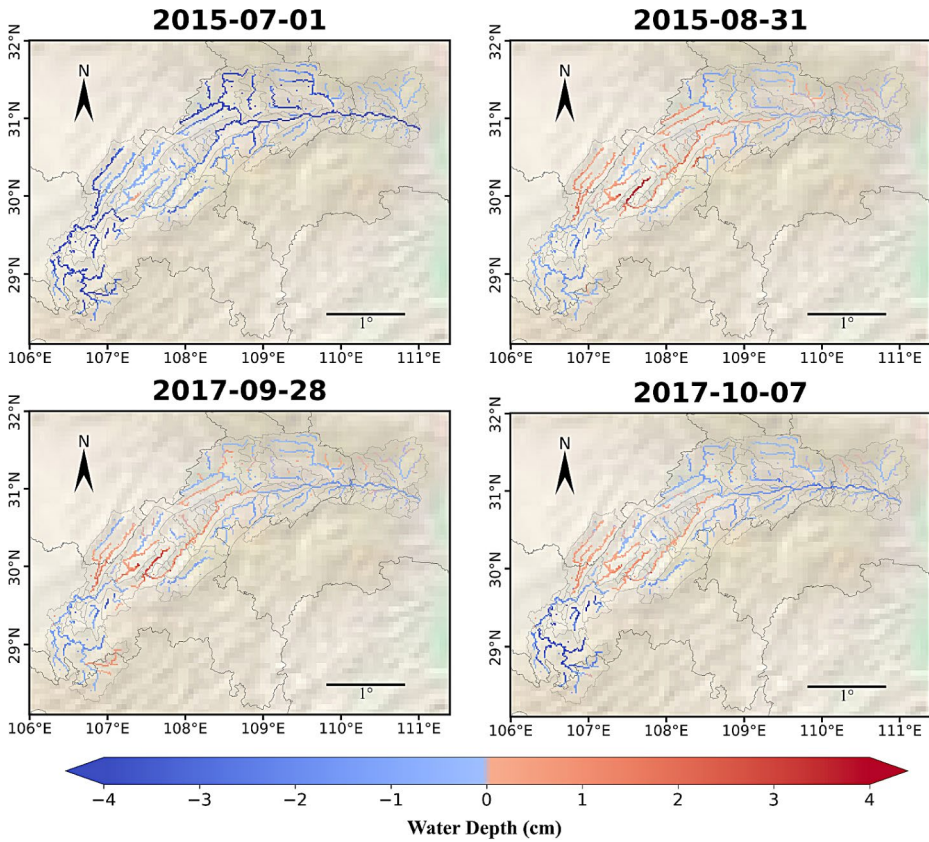


Fig. 7 Difference in water depth between LUC2015 and LUC2020 scenarios in flood events 1,7,8,9 (Note: water depth map is at 1-min, and water depth has not changed is not represented in the figure)

In LUC2015 scenarios, the average water depth was reduced by 0.03% in flood event 7 (peaked on 08/31/2017) compared with LUC2020, and the maximum water depth was 22.40% higher. For flood event 8 (peaked on 09/28/2017), the average water depth was reduced by 0.07% compared with LUC2020, and the maximum water depth was 32.30% higher. Increased water depth was found in the river section from Changshou to Shuangjiang Station in the mainstream of the Yangtze River and the Yulinhe, Longxihe, and Quxi basin. In contrast, the Qijiang, Wubuhe, Lixiangxi basin, and the northwest region of the TGR were found to have decreased water depth.

For Flood Event 9 (peaked on 10/07/2017), the distribution of water depth difference is similar to Flood Events 7 and 8. In LUC2015 scenarios, the average water depth was reduced by -0.64% compared with LUC2020, and the maximum water depth was over 1000% higher. The maximum water depth difference is 4.71 cm.

4 Discussions

4.1 Comparison with previous studies

Previous studies revealed the flow trend in UYR (Upper Yangtze River, including the TGR and the upstream region), and explained the reasons for this decline due to climate change, human water consumption, and reservoir impoundment (Wei et al. 2014; Shi et al. 2022). According to our results, both the runoff and water depth in the TGRR and the UYR exhibited an increasing trend in 2015–2018 which could be attributed to precipitation anomaly. According to our result, streamflow during summer and autumn was characterized by decreasing trends and increasing trends in spring and winter, which is consistent with previous studies (Jiang et al. 2008; Huang et al. 2024). Furthermore, this study reveals that water depth shows the same seasonal pattern.

Previous studies have attempted to reflect hydrological conditions by analyzing only streamflow change in the TGRR, while this study provides a comprehensive evaluation of streamflow and water depth to reflect flood security conditions. Compared to past research (Wang et al. 2019b; Cheng et al. 2024), this study enables the reflection of flooding dynamics of the TGRR explicitly by the flood depth map. Some studies also turned their views on flood dynamics by applying hydrological-hydrodynamic models, while, currently the use one-dimensional hydrodynamic model limited the knowledge (Wang et al. 2003; Zhang et al. 2020). In this study, by introducing the 2D hydrodynamic model, this study could take flood depth mapping that explicitly reflects flood heterogeneity. This method has been widely adopted in previous studies in the LMRB and other basins to reflect flood dynamics (Kim et al. 2021; Sun et al. 2024).

The impoundment and land cover changes impact hydrologic processes (Wang et al. 2019a). This study assessed the impact of LUCC on hydrological features in TGRR by designing scenarios. During the period spanning from 2015 to 2020, notable land cover changes within the TGRR, attributed to urbanization and the Cropland to Forest Conversion policy, include an increase in urban and built-up areas (+0.6%) and water bodies (+0.1%), a decrease in woodland-grassland (-0.7%) and cropland (-0.1%). This led to slight increasing runoff and inflow of the TGR, and reduced daily mean and maximum water depth in this whole region (particularly in the flood seasons). In addition, the water depth difference between LUCC2015 and LUCC2020 scenarios shows evident spatial variations and it varies with flood events. Reductions in water depth are observed in the northeast region (s.t. Qijiang, Wubuhe, Lixiangxi basins), particularly in the river section from Cuntan Station to Qingxi Field Station in the mainstream of the Yangtze River. Conversely, increased water depth during LUCC is noted in the northern region (Yulin, Xiaojiang, and Huangjin subbasins).

4.2 Impacts of LUCC on hydrological processes in the TGRR

The “Grain for Green Project” is a country-wide ecological program to convert marginal cropland to forest, which has been implemented in China since 2002. As an important ecological zone, the TGRR has adopted this policy to reserve forest resources and ecological carrying capacity. Previous research discussed the impact of policy implementation which leads to increasing vegetation on hydrological processes (Han et al. 2022; Lan et al. 2024).

In the Guansihe basin in Mianyang, Sichuan province, cropland conversion to forests significantly decreased runoff (Yu et al. 2015). Increased significantly vegetation cover area due to the implementation of the GGP leads to reducing blue water and surface runoff while increasing green water (Han et al. 2022). Large-scale vegetation greening leads to national hydrological drought (Lan et al. 2024). Contrastingly, the arid Loess Plateau experienced a decreasing runoff after this measure's implementation, while the flow in the upper and middle sub-basins increased by about 15% and 20% (Qiu et al. 2011).

In this study, based on 2015 and 2020 land use data, this study designed scenarios with different land uses and analyzed the effect of land use change on streamflow and water depth. Results showed that land use change in the area led to increasing runoff, as opposed to previous studies. Expanding construction land may explain this trend: from 2015 to 2020, the region witnessed the most rapid urban development, and the most noticeable change in land use was a conversion of cropland and grassland to urban. Also, the dominant cover type changed from cropland to urban and built-up in the Changtang River basin. There are three subbasins where the main land cover type changes from cropland to grassland, urban area, grassland to cropland. As a result, despite the growing forest leading to a redistribution of surface and subsurface runoff and a subsequent decrease in runoff volume, the expansion of impervious surfaces within the interval overwhelmed these effects, resulting in increasing runoff (Zhou et al. 2013).

4.3 Limitations and applicability

This study tested responses of hydrologic variables to land use change and changing climate, yet there remains room for improvement. To enhance the precision of simulating hydrological characteristics within the TGRR, future studies could incorporate precise rainfall data with higher resolution, both temporally and spatially. While calibrated models yielded satisfactory results and parameter uncertainty was estimated, it should be emphasized that the calibration methods used in this study were relatively simple. Adapting state-of-the-art calibration techniques could lead to better performance. Furthermore, collecting data from more hydrological stations and long periods could significantly improve regional parameter estimation. In this study, the assessment of simulated water depth is qualitative, and the focus remains on investigating relative water depth both in time and space. Obtaining the topographic data of the measured area to calibrate the hydrodynamic model (including hydraulic parameters) can obtain a finer and more accurate distribution of bathymetry within the region and enable the quantitative analysis of water depth during flood events. Despite the limitations, this study could reflect changes in streamflow and water depth during 2014–2018 and assess flood security conditions in the context of climate change, LUCC, and rapid urbanization.

Coupling hydrological-hydrodynamic models to simulate hydrological characteristics and reflect flood dynamics can be adopted in other regions. It's noted that considering that runoff is an important input that determines simulation performance. In this study, VIC is selected considering that it is suitable in humid basins, and has been examined its validity in this region. the hydrological model selection and parameter estimation are essential.

5 Conclusions

Runoff in the TGR has a significant impact on the flood control and safety of the Yangtze River basin. However, due to the lack of measured data in the region, the understanding of the hydrological characteristics of this region is limited. In this study, the hydrological characteristics of the TGR are simulated using the VIC and CaMa-Flood models. Calibrated parameters performed reasonably well in representing the natural and observed discharge in the region. The NSE for daily discharge is 0.81, R_e is -2%, and the R-square is 0.93. Simulations mostly overestimated the peak flows (relative error ranges from -2.5 to 40.0%), and the bias in flood peak occurrence time is 2 to -5 days.

Increasing rates of monthly average, maximum, and minimum flow were 124.56–8.40 m³/s/a from 2015 to 2018. The monthly average flow exhibits a seasonal trend, initially increasing and later decreasing throughout the year, aligning with observations at Yichang station. Results show an increase in runoff in the TGR during 2015–2018, accompanied by a decrease in runoff during the flood season (-146.47 m³/s/a~87.60 m³/s/a). Between 2015 and 2018, the TGR observed an increase in water depth, with change rates for the average depth spanning from 0.11 cm/a to 0.47 cm/a and for the maximum depth, fluctuating between 0.08 m/a and 0.34 m/a. While flood season saw a decrease in average water depth, change rates varied from -0.21 cm/a to -0.61 cm/a.

Based on 2015 and 2020 land use data, this study designed scenarios with different land use maps. From 2015 to 2020, the region witnessed the most noticeable change in land use was a conversion of cropland and grassland to urban. The dominant cover type changed from cropland to urban and built-up in the Changtang River basin. There are three subbasins where the main land cover type changes from cropland to grassland, urban area, grassland to cropland. Results showed that land use change caused a slight increase in runoff and a 7.70% decrease in the multi-year average water depth, while an increase in water depth was observed in the northern TGR.

Supplementary Information The online version contains supplementary material available at <https://doi.org/10.1007/s11069-024-06870-0>.

Acknowledgements The authors thank the VIC team and the CaMa-Flood teams for providing the model. Our cordial gratitude should be extended to the editor, Prof. Dr. John Clague, and anonymous reviewers for their pertinent and professional comments and suggestions which are greatly helpful for further quality improvement of this manuscript.

Author contributions YS contributed to the conceptualization; formal analysis; methodology and original version of the manuscript. QZ contributed to the conceptualization; Funding acquisition; Project administration; Resources; Supervision; Writing-review & editing. WS contributed to the Funding acquisition; Project administration; Resources; Writing-review. ST contributed to the visualization and methodology; VS contributed to the Writing-review & editing and overall improvement of the quality of this manuscript.

Funding This work was funded by the Three Gorges Follow-up Work “Remote Sensing Investigation and Evaluation of Flood Control Safety in the Three Gorges Section”, grant number JZ0161A012023.

Data availability The data presented in this study are available upon request from the corresponding author.

Declarations

Competing interests The authors have no relevant financial or non-financial interests to disclose.

References

- Alizadeh Z, Yazdi J (2023) Calibration of hydrological models for ungauged catchments by automatic clustering using a differential evolution algorithm: the Gorganrood river basin case study. *J Hydroinformatics* 25:645–662. <https://doi.org/10.2166/hydro.2023.081>
- Brookfield AE, Ajami H, Carroll RWH et al (2023) Recent advances in integrated hydrologic models: integration of new domains. *J Hydrol* 620:129515. <https://doi.org/10.1016/j.jhydrol.2023.129515>
- Burgan Hİ, İçağa Y, Bostanoğlu Y, Kilit M (2013) Water quality tendency of Akarçay river between 2006–2011. *Pamukkale Univ J Eng Sci* 19:127–132. <https://doi.org/10.5505/pajes.2013.46855>
- Cheng J, Xu L, Fan H, Jiang J (2019) Changes in the flow regimes associated with climate change and human activities in the Yangtze River. *River Res Appl* 35:1415–1427. <https://doi.org/10.1002/rra.3518>
- Cheng H, Wang T, Yang D (2024) Quantifying the regulation capacity of the Three Gorges Reservoir on extreme hydrological events and its impact on flow regime in a changing climate. *Water Resour Res* 60:e2023WR036329. <https://doi.org/10.1029/2023WR036329>
- Donat MG, Lowry AL, Alexander LV et al (2016) More extreme precipitation in the world's dry and wet regions. *Nat Clim Change* 6:508–513. <https://doi.org/10.1038/nclimate2941>
- Elmer NJ, McCreight J, Hain C (2021) Hydrologic model parameter estimation in ungauged basins using simulated SWAT discharge observations. *Water Resour Res* 57. <https://doi.org/10.1029/2021WR029655>. e2021WR029655
- Fang J, Kong F, Fang J, Zhao L (2018) Observed changes in hydrological extremes and flood disaster in Yangtze River Basin: spatial-temporal variability and climate change impacts. *Nat Hazards* 93:89–107. <https://doi.org/10.1007/s11069-018-3290-3>
- FAO/IIASA/ISRIC/ISSCAS/JRC (2012) Harmonized World Soil Database (version 1.2). Available online: <http://webarchive.iiasa.ac.at/Research/LUC/External-World-soil-database/HTML/> (accessed on 27 December 2023)
- Gong L, Zhang X, Pan G et al (2023) Hydrological responses to co-impacts of climate change and land use/cover change based on CMP6 in the Ganjiang River, Poyang Lake Basin. *Anthropocene* 41:100368. <https://doi.org/10.1016/j.ancene.2023.100368>
- Gründemann GJ, van de Giesen N, Brunner L, van der Ent R (2022) Rarest rainfall events will see the greatest relative increase in magnitude under future climate change. *Commun Earth Environ* 3:1–9. <https://doi.org/10.1038/s43247-022-00558-8>
- Gu H, Yu Z, Wang G et al (2015) Impact of climate change on hydrological extremes in the Yangtze River Basin, China. *Stoch Environ Res Risk Assess* 29:693–707. <https://doi.org/10.1007/s00477-014-0957-5>
- Han Y, Xia F, Huang H et al (2022) Impact of the grain for Green Project on water resources and ecological water stress in the Yanhe River Basin. *PLoS ONE* 17:e0259611. <https://doi.org/10.1371/journal.pone.0259611>
- Hansen MC, Defries RS, Townshend JRG, Sohlberg R (1999) Global Land Cover Facility. University of Maryland Institute for Advanced Computer Studies, College Park, Maryland, U.S.A., 1km global land cover dataset derived from AVHRR
- Hansen MC, Defries RS, Townshend JRG, Sohlberg R (2000) Global land cover classification at 1 km spatial resolution using a classification tree approach. *Int J Remote Sens* 21:1331–1364. <https://doi.org/10.1080/014311600210209>
- Hirabayashi Y, Mahendran R, Koirala S et al (2013) Global flood risk under climate change. *Nat Clim Change* 3:816–821. <https://doi.org/10.1038/nclimate1911>
- Hrachowitz M, Savenije HHG, Blöschl G et al (2013) A decade of predictions in Ungauged basins (PUB)—a review. *Hydrol Sci J* 58:1198–1255. <https://doi.org/10.1080/02626667.2013.803183>
- Huang C, Zhou Z, Teng M et al (2020) Effects of climate, land use and land cover changes on soil loss in the Three Gorges Reservoir area, China. In: *Geography and Sustainability*, pp 200–208
- Huang A, Gao G, Yao L et al (2024) Spatiotemporal variations of inter- and intra-annual extreme streamflow in the Yangtze River Basin. *J Hydrol* 629:130634. <https://doi.org/10.1016/j.jhydrol.2024.130634>
- Hurkmans RTWL, Terink W, Uijlenhoet R et al (2009) Effects of land use changes on streamflow generation in the Rhine basin. *Water Resour Res* 45. <https://doi.org/10.1029/2008WR007574>
- Jiang T, Kundzewicz ZW, Su B (2008) Changes in monthly precipitation and flood hazard in the Yangtze River Basin, China. *Int J Climatol* 28:1471–1481. <https://doi.org/10.1002/joc.1635>
- Jing L, Zhang X, Wang J, Cheng H (2004) Application of GIS in simulation of river basin hydrology in Three Gorges Project reservoir. *J Hydraul Eng* 677–681
- Jongman B, Ward PJ, Aerts JCJH (2012) Global exposure to river and coastal flooding: long term trends and changes. *Glob Environ Change* 22:823–835. <https://doi.org/10.1016/j.gloenvcha.2012.07.004>

- Ju F, An R, Yang Z et al (2020) Assimilating SMOS brightness temperature for hydrologic model parameters and soil moisture estimation with an immune evolutionary strategy. *Remote Sens* 12:1556. <https://doi.org/10.3390/rs12101556>
- Kim S, Shen H, Noh S et al (2021) High-resolution modeling and prediction of urban floods using WRF-Hydro and data assimilation. *J Hydrol* 598:126236. <https://doi.org/10.1016/j.jhydrol.2021.126236>
- Lan X, Xie Y, Liu Z et al (2024) Vegetation greening accelerated hydrological drought in two-thirds of river basins over China. *J Hydrol* 637:131436. <https://doi.org/10.1016/j.jhydrol.2024.131436>
- Li Y, Piao S, Li LZ et al (2018) Divergent hydrological response to large-scale afforestation and vegetation greening in China. *Sci Adv* 4:eaar4182. <https://doi.org/10.1126/sciadv.aar4182>
- Li C, Sun G, Caldwell PV et al (2020) Impacts of urbanization on watershed water balances across the conterminous United States. <https://doi.org/10.1029/2019WR026574>
- Liang X, Xie Z (2001) A new surface runoff parameterization with subgrid-scale soil heterogeneity for land surface models. *Adv Water Resour* 24:1173–1193. [https://doi.org/10.1016/S0309-1708\(01\)00032-X](https://doi.org/10.1016/S0309-1708(01)00032-X)
- Liang X, Lettenmaier DP, Wood EF, Burges SJ (1994) A simple hydrologically based model of land surface water and energy fluxes for general circulation models. *J Geophys Res Atmos* 99:14415–14428. <https://doi.org/10.1029/94JD00483>
- Lin H, Pan J, Zou H (2022) Real-time forecast of urban flood in China: past, present and future. *Acta Geod Cartogr Sin*. <https://doi.org/10.11947/j.AGCS.2022.20220144>
- Liu J, Kuang W, Zhang Z et al (2014) Spatiotemporal characteristics, patterns, and causes of land-use changes in China since the late 1980s. *J Geogr Sci* 24:195–210. <https://doi.org/10.1007/s11442-014-1082-6>
- Lohmann D, Nolte-Holube R, Raschke E (1996) A large-scale horizontal routing model to be coupled to land surface parametrization schemes. *Tellus A* 48:708–721. <https://doi.org/10.1034/j.1600-0870.1996.t01-3-00009.x>
- Lu W, Wang W, Shao Q et al (2018) Hydrological projections of future climate change over the source region of Yellow River and Yangtze River in the Tibetan Plateau: a comprehensive assessment by coupling RegCM4 and VIC Model. *Hydrol Process* 32:2096–2117. <https://doi.org/10.1002/hyp.13145>
- Luo K, Zhang X (2022) Increasing urban flood risk in China over recent 40 years induced by LUCC. *Landsc Urban Plan* 219:104317. <https://doi.org/10.1016/j.landurbplan.2021.104317>
- Moriasi D, Arnold J, Van Liem M et al (2007) Model evaluation guidelines for systematic quantification of accuracy in watershed simulations. *Trans ASABE* 50:885–900. <https://doi.org/10.13031/2013.23153>
- Moriasi D, Gitau M, Pai N, Daggupati P (2015) Hydrologic and water quality models: performance measures and evaluation criteria. *Trans ASABE* 58:1763–1785. <https://doi.org/10.13031/trans.58.10715>
- Moustakis Y, Papalexioiu SM, Onof CJ, Paschalis A (2021) Seasonality, intensity, and duration of rainfall extremes change in a warmer climate. *Earths Future* 9. <https://doi.org/10.1029/2020EF001824>. e2020EF001824
- Myhre G, Alterskjær K, Stjern CW et al (2019) Frequency of extreme precipitation increases extensively with event rareness under global warming. *Sci Rep* 9:16063. <https://doi.org/10.1038/s41598-019-52277-4>
- Pang S, Xu J (2012) Discussion on flood forecast method by distributed hydrological model combining with meteorological forecast data: case of real - time flood forecast of three gorges region. <https://doi.org/10.3969/j.issn.1001-4179.2012.03.017>. Yangtze River 43:
- Pang S, Chen R, Peng, Fu et al (2022) Analysis of water level and flow of Yichang station in dry season considering the influence of water conservancy projects. *Hydropower New Energy* 36:14–17. <https://doi.org/10.13622/j.cnki.cn42-1800/tv.1671-3354.2022.11.004>
- Park D, Markus M (2014) Analysis of a changing hydrologic flood regime using the variable infiltration capacity model. *J Hydrol* 515:267–280. <https://doi.org/10.1016/j.jhydrol.2014.05.004>
- Qiu GY, Yin J, Tian F, Geng S (2011) Effects of the Conversion of Cropland to Forest and Grassland Program on the Water Budget of the Jinghe River Catchment in China. *J Environ Qual* 40:1745–1755. <https://doi.org/10.2134/jeq2010.0263>
- Rodell M, Li B (2023) Changing intensity of hydroclimatic extreme events revealed by GRACE and GRACE-FO. *Nat Water* 241–248. <https://doi.org/10.1038/s44221-023-00040-5>
- Shen Z, Qiu J, Hong Q, Chen L (2014) Simulation of spatial and temporal distributions of non-point source pollution load in the Three Gorges Reservoir Region. *Sci Total Environ* 493:138–146. <https://doi.org/10.1016/j.scitotenv.2014.05.109>
- Shi R, Wang T, Yang D, Yang Y (2022) Streamflow decline threatens water security in the upper Yangtze river. *J Hydrol* 606:127448. <https://doi.org/10.1016/j.jhydrol.2022.127448>
- Shin S, Pokhrel Y, Yamazaki D et al (2020) High resolution modeling of river-floodplain-reservoir inundation dynamics in the Mekong River Basin. *Water Resour Res* 56. <https://doi.org/10.1029/2019WR026449>. e2019WR026449
- Sood A, Smakhtin V (2015) Global hydrological models: a review. *Hydrol Sci J* 60:549–565. <https://doi.org/10.1080/02626667.2014.950580>

- Sun Y, Zhang Q, Singh VP (2024) Flooding in the Yellow River Basin, China: spatiotemporal patterns, drivers and future tendency. *J Hydrol Reg Stud* 52:101706. <https://doi.org/10.1016/j.ejrh.2024.101706>
- Wang J (2021) Flood forecasting of the Three Gorges Intervening Basin based on the coupling of meteorology and hydrology. Dalian University of Technology
- Wang Y, Yang X (2020) A coupled hydrologic–hydraulic model (XAJ–HiPIMS) for flood simulation. *Water* 12:1288. <https://doi.org/10.3390/w12051288>
- Wang C, Guo L, Rui X, Kong F (2003) Study on real time flood forecasting system for the Three Gorges Reservoir. *Adv Water Sci* 14. <https://doi.org/10.3321/j.issn:1001-6791.2003.06.001>
- Wang B, Tian F, Hu H (2011a) Analysis of the effect of regional lateral inflow on the flood peak of the Three Gorges Reservoir. *Sci China Technol Sci* 41:914–923. <https://doi.org/10.1007/s11431-011-4330-3>
- Wang B, Zhe L, Tian F, Yang D (2011b) Physically distributed hydrological model simulations of runoff in the Three Gorges Region. *J Tsinghua Univ Sci Technol* 51. <https://doi.org/10.16511/j.cnki.qhdxxb.2011.02.024>
- Wang K, Zhang Q, Chen YD, Singh VP (2015) Effects of land-use/cover change on hydrological processes using a GIS/RS-based integrated hydrological model: case study of the East River, China. *Hydrol Sci J* 60:1724–1738. <https://doi.org/10.1080/02626667.2014.949723>
- Wang H, Xiao W, Zhao Y et al (2019a) The spatiotemporal variability of evapotranspiration and its response to climate change and land use/land cover change in the Three Gorges Reservoir. *Water* 11:1739. <https://doi.org/10.3390/w11091739>
- Wang W, Zhu Y, Dong S et al (2019b) Attribution of decreasing annual and autumn inflows to the Three Gorges Reservoir, Yangtze River: climate variability, water consumption or upstream reservoir operation? *J Hydrol* 579:124180. <https://doi.org/10.1016/j.jhydrol.2019.124180>
- Wang Q, Xu Y, Wang Y et al (2020) Individual and combined impacts of future land-use and climate conditions on extreme hydrological events in a representative basin of the Yangtze River Delta, China. *Atmospheric Res* 236:104805. <https://doi.org/10.1016/j.atmosres.2019.104805>
- Wang J, Yun X, Pokhrel Y et al (2021) Modeling daily floods in the Lancang-Mekong River Basin using an improved hydrological-hydrodynamic model. *Water Resour Res* 57. <https://doi.org/10.1029/2021WR029734>. e2021WR029734
- Wei W, Chang Y, Dai Z (2014) Streamflow changes of the Changjiang (Yangtze) River in the recent 60 years: impacts of the east Asian summer monsoon, ENSO, and human activities. *Quat Int* 336:98–107. <https://doi.org/10.1016/j.quaint.2013.10.064>
- Willner SN, Levermann A, Zhao F, Frieler K (2018) Adaptation required to preserve future high-end river flood risk at present levels. *Sci Adv* 4:eaa01914. <https://doi.org/10.1126/sciadv.aao1914>
- Winsemius H, Aerts J, van Beek L, Bierkens MFP (2016) Global drivers of future river flood risk. *Nat Clim Change* 6:381–385. <https://doi.org/10.1038/nclimate2893>
- Xia J, Chen J (2021) A new era of flood control strategies from the perspective of managing the 2020 Yangtze River flood. *Sci China Earth Sci* 64:1–9. <https://doi.org/10.1007/s11430-020-9699-8>
- Xie Z, Yuan F, Duan Q et al (2007) Regional parameter estimation of the VIC land surface model: methodology and application to river basins in China. *J Hydrometeorol* 8:447–468. <https://doi.org/10.1175/JHM568.1>
- Xu X, Liu J, Zhang R et al (2018) China's multi-period land Use Land Cover remote sensing monitoring data set (CNLUCC). Resource and Environment Data Cloud Platform
- Xu C, Han Z, Fu H (2022) Remote sensing and hydrologic-hydrodynamic modeling integrated approach for rainfall-runoff simulation in farm dam dominated basin. *Front Environ Sci* 9. <https://doi.org/10.3389/fenvs.2021.817684>
- Yamazaki D, Kanae S, Kim H, Oki T (2011) A physically based description of floodplain inundation dynamics in a global river routing model. *Water Resour Res* 47. <https://doi.org/10.1029/2010WR009726>
- Yamazaki D, de Almeida, Bates PD, Gustavo AM (2013) Improving computational efficiency in global river models by implementing the local inertial flow equation and a vector-based river network map. *Water Resour Res* 49:7221–7235. <https://doi.org/10.1002/wrcr.20552>
- Yamazaki D, Sato T, Kanae S et al (2014) Regional flood dynamics in a bifurcating mega delta simulated in a global river model. *Geophys Res Lett* 41:3127–3135. <https://doi.org/10.1002/2014GL059744>
- Yamazaki D, Ikeshima D, Sosa J et al (2019) MERIT Hydro: a high-resolution global hydrography map based on latest topography dataset. *Water Resour Res* 55:5053–5073. <https://doi.org/10.1029/2019WR024873>
- Yang SL, Xu KH, Milliman JD et al (2015) Decline of Yangtze River water and sediment discharge: impact from natural and anthropogenic changes. *Sci Rep* 5:12581. <https://doi.org/10.1038/srep12581>
- Yu F, Chen Z, Ren X, Yang G (2009) Analysis of historical floods on the Yangtze River, China: characteristics and explanations. *Geomorphology* 113:210–216. <https://doi.org/10.1016/j.geomorph.2009.03.008>
- Yu P, Wang Y, Coles N et al (2015) Simulation of runoff changes caused by cropland to forest conversion in the Upper Yangtze River Region, SW China. *PLoS ONE* 10:e0132395. <https://doi.org/10.1371/journal.pone.0132395>

- Zeng F, He Q, Li Y et al (2024) Reduced runoff in the upper Yangtze River due to comparable contribution of anthropogenic and climate changes. *Earths Future* 12. <https://doi.org/10.1029/2023EF004028>. e2023EF004028
- Zhang Q, Lou Z (2011) The environmental changes and mitigation actions in the Three Gorges Reservoir region, China. *Environ Sci Policy* 14:1132–1138. <https://doi.org/10.1016/j.envsci.2011.07.008>
- Zhang Q, Li J, Singh VP, Xiao M (2013) Spatio-temporal relations between temperature and precipitation regimes: implications for temperature-induced changes in the hydrological cycle. *Glob Planet Change* 111:57–76. <https://doi.org/10.1016/j.gloplacha.2013.08.012>
- Zhang L, Nan Z, Yu W, Ge Y (2015) Modeling land-use and Land-Cover change and hydrological responses under consistent climate change scenarios in the Heihe River Basin, China. *Water Resour Manag* 29:4701–4717. <https://doi.org/10.1007/s11269-015-1085-9>
- Zhang L, Lu J, Chen X et al (2017) Stream flow simulation and verification in ungauged zones by coupling hydrological and hydrodynamic models: a case study of the Poyang Lake ungauged zone. *Hydrol Earth Syst Sci* 21:5847–5861. <https://doi.org/10.5194/hess-21-5847-2017>
- Zhang Z, Zhang Q, Singh VP (2018a) Univariate streamflow forecasting using commonly used data-driven models: literature review and case study. *Hydrol Sci J* 63:1091–1111. <https://doi.org/10.1080/02626666.7.2018.1469756>
- Zhang Z, Zhang Q, Singh VP, Shi P (2018b) River flow modelling: comparison of performance and evaluation of uncertainty using data-driven models and conceptual hydrological model. *Stoch Environ Res Risk Assess* 32:2667–2682. <https://doi.org/10.1007/s00477-018-1536-y>
- Zhang Y, Zhou J, Lu C (2020) Integrated hydrologic and hydrodynamic models to improve flood simulation capability in the data-scarce Three Gorges Reservoir Region. *Water* 12:1462. <https://doi.org/10.3390/w12051462>
- Zhou S, Liang X, Chen J, Gong P (2004) An assessment of the VIC-3L hydrological model for the Yangtze River basin based on remote sensing: a case study of the Baohe River basin. *Can J Remote Sens* 30:840–853
- Zhou F, Xu Y, Chen Y et al (2013) Hydrological response to urbanization at different spatio-temporal scales simulated by coupling of CLUE-S and the SWAT model in the Yangtze River Delta region. *J Hydrol* 485:113–125. <https://doi.org/10.1016/j.jhydrol.2012.12.040>

Publisher's Note Springer Nature remains neutral with regard to jurisdictional claims in published maps and institutional affiliations.

Springer Nature or its licensor (e.g. a society or other partner) holds exclusive rights to this article under a publishing agreement with the author(s) or other rightsholder(s); author self-archiving of the accepted manuscript version of this article is solely governed by the terms of such publishing agreement and applicable law.